Case Studies in Thermal Engineering 44 (2023) 102863

Contents lists available at ScienceDirect

Case Studies in Thermal Engineering

journal homepage: www.elsevier.com/locate/csite

Performance evaluation of a hydrogen-fired combined cycle with water recovery

Tingting Wei, Zhenchao Hu, Xingyu Tang, Huisheng Zhang *

The Key Laboratory of Power Machinery and Engineering of Education Ministry, Shanghai Jiao Tong University, Shanghai, 200240, PR China

HIGHLIGHTS

- A new water recycling scheme is proposed for the hydrogen-fired combined cycle.
- A modular modeling is used with water recovery condenser and exhaust gas blower.
- A new evaluation model is established using performance and economic indices.
- The hydrogen-fired combined cycle was more efficient than natural-gas-fired ones.
- The scheme with water recovery provides environmental and economic benefits.

GRAPHICAL ABSTRACT

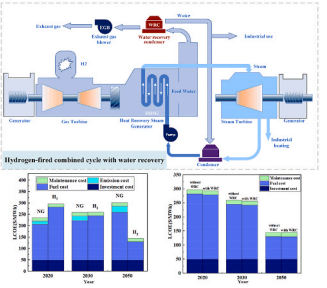

ARTICLE INFO

Keywords:
Hydrogen combustion
Combined cycle
Water recovery
Performance analysis
Gas turbine

ABSTRACT

Hydrogen can alleviate the increasing environmental pollution and has good development prospects in power generation due to its high calorific value and low environmental impact. The previously designed hydrogen-fired combined cycle ignored water recycling, which led to an inefficient application of hydrogen and the wastage of water. This paper proposes the concept of a hydrogen-fired combined cycle with water recovery to reuse the condensed water as an industrial heat supply. It was applied to an F-class combined cycle power plant. The results demonstrate that the efficiency of hydrogen-fired combined cycles with and without water recovery increased by 1.92% and 1.35%, respectively, compared to that of the natural-gas-fired combined cycle under full working conditions. In addition, an economic comparison of the three cycles was conducted. The levelized cost of energy of the hydrogen-fired combined cycle with water recovery will be 52.22% lower than that of the natural-gas-fired combined cycle in 2050. This comparative study suggested that water recovery supplementation could improve the gas turbine efficiency. The

* Corresponding author.
E-mail address: zhslm@sjtu.edu.cn (H. Zhang).

https://doi.org/10.1016/j.csite.2023.102863
Received 20 October 2022; Received in revised form 23 February 2023; Accepted 25 February 2023
Available online 4 March 2023
2214-157X/© 2023 The Authors. Published by Elsevier Ltd. This is an open access article under the CC BY-NC-ND license (http://creativecommons.org/licenses/by-nc-nd/4.0/).

proposed hydrogen-fired combined cycle with water recovery would provide both environmental and economic benefits.

1. Introduction

Global climate change and energy shortages are accelerating the energy transition, resulting in the widespread use of clean energy. The hydrogen industry has received increasing attention from countries such as Germany, the United States, and Japan because of its high calorific value and pollution-free combustion products. These countries have successively introduced practical hydrogen strategies to facilitate its development [1]. Furthermore, China has announced its goal of achieving carbon neutrality by 2060 [2]. This declaration has promoted the development of the hydrogen industry in China, including hydrogen power generation. In recent years, the gas turbine combined cycle (GTCC), usually using natural gas as a fuel, has been essential to power generation in China. If natural gas is gradually replaced by hydrogen by upgrading gas turbines (GTs), carbon emissions would be reduced.

GTs have been evolving toward decreasing pollutant emissions [3,4]. Two methods are often implemented to reduce the environmental damage caused by sulfur dioxide (SO_2) from coal-fired power plants: one is to scrub SO_2 from the exhaust gas, and the other is to generate syngas (i.e., a mixture of carbon monoxide and hydrogen) from coal. Given the impact of nitrogen oxides (NO_x) on the natural environment and human health, coal-fired power plants adopt selective catalytic reduction or low-NO_x burners to lower NO_x emissions. There are two typical modes for obtaining low-NO_x burners (i) water or steam injection in diffusion burners (i.e., wet low emissions): and (ii) use of segmented and lean premixed combustion technology to build new dry low emission (DLE) burners. In addition, two methods have been presented to reduce carbon dioxide (CO_2) emissions to curb global warming: one is post-combustion capture, also termed CO_2 washing, and the other is pre-combustion capture by generating hydrogen from renewable energy sources and traditional fossil energy.

There are two research directions in this field: concept improvement and realistic applications. Some scholars have improved the basic concept of the combined cycle theoretically to substitute fossil fuels with hydrogen. Early in 1976, Vanco [5] analyzed the thermodynamics and turbine characteristics of turbine-driven hydrogen-fueled auxiliary space power systems. Forsberg [6] proposed a nuclear–hydrogen combined cycle to meet the spinning reserve requirements and stabilize the grid. Because nuclear heat raises air temperatures above the auto-ignition temperature of the hydrogen and powers the air compressor, the power output can be varied rapidly, unlike with fossil-fired turbines. Jericha et al. [7] presented a hybrid plant that incorporated solid oxide fuel cells into an innovative power cycle with steam as the working fluid. Toja-Silva and Rovira [8] presented an analysis based on the first and second laws of thermodynamics to investigate the efficiency of a hydrogen/oxygen-fueled GT, which produced both electrical and thermal energy. The Graz Cycle, proposed by Jericha of the Technical University of Graz, is an original combination of the Joule and Rankine cycles. In 2018, his team adapted the Graz Cycle for hydrogen combustion with pure oxygen [9]. Arsalis [10] presented a detailed thermodynamic model of a small-scale natural gas/hydrogen-fueled GT system. Ditaranto et al. [11] investigated the use of a hydrogen-fired GT cycle with exhaust gas recirculation (EGR) to control NO formation. Görgülü et al. [12] analyzed the changes in the performances of GTs due to water injection into the air before the compressor. Koç et al. [13] calculated the power production and the thermal and exergy efficiencies for simple and recuperative GT cycles. Petersen et al. [14,15] analyzed the thermodynamic performance, emission reduction potential, and combustion stability limits of a hydrogen-fired GT with external exhaust gas recirculation.

In realistic applications, some specific issues need to be solved when replacing natural gas with hydrogen in the GTCC [16–18], such as flashback and flame oscillation, auto-ignition of pure hydrogen at high temperatures and pressures, and modification of the combustion chamber (CC) structure. To remedy these issues, Chiesa et al. [16] proposed three strategies to moderately re-design heavy-duty GTs to switch from natural gas to diluted hydrogen. Cappelletti and Martelli [19] modified an existing heavy-duty GT burner and carried out investigations on a lean premixed burner with 100% hydrogen supplied. Schastlivtsev et al. [20] presented a hydrogen–oxygen gas generator to store energy in both compressed air and hydrogen. In addition, GT manufacturers are developing a hydrogen-fired combined cycle. Currently, these manufacturers focus on various technological developments such as natural gas and hydrogen co-fired GTs, pure hydrogen burners, and DLE combustors [21–23]. The Fusina hydrogen power station, located in Italy and operated by Enel, is the world's first commercial-scale power station fueled by pure hydrogen [24].

Overall, various improvements have been made to the hydrogen-fired combined cycle by analyzing its thermal performance, economics, or pollutant emissions; almost all of these focus on methods such as dry EGR, wet EGR, and water injection, and there is still some space for research, outlined in what follows. 1) Compared with wet combustion, DLE combustion decreases the use of industrial water and extends the blade life. Hence, the development of hydrogen-rich or even pure hydrogen DLE burners is a future research direction in GT power generation. 2) Most established simulation models are relatively simple because of the unrefined modeling. For instance, the heat recovery steam generator (HRSG) is set as an integrated component in models. 3) The exhaust gas is directly discharged in the current circulation concept. This concept ignores the water produced by hydrogen combustion, leading to extensive losses to the power plant. The widespread use of hydrogen fuel could have environmental impacts due to unintended emissions of molecular hydrogen [25]. Therefore, it is necessary to extract the water from the exhaust gas for recycling, rather than discharging it at will.

In this paper, the concept of a hydrogen-fired combined cycle with water recovery is proposed. In contrast to existing cycles, the pure hydrogen DLE combustion system is adopted in this proposed concept. Furthermore, a water recovery condenser (WRC) and an exhaust gas blower (EGB) are attached to the outlet of the HRSG to recover the water from the exhaust gas for water supplementation and other industrial uses. It is assumed that the boundary conditions and component characteristics of this cycle are the same as those

of an actual natural-gas-fired power plant. The operating data of the natural-gas-fired power plant are taken as a reference when establishing the hydrogen-fired model. Comparative studies showed that the presented work can promote energy efficiency, avoid the wastage of industrial water, and mitigate the effects of elemental hydrogen on the environment.

2. Concept of hydrogen-fired combined cycle with water recovery

Hydrogen can provide deep decarbonization for traditional industries (e.g., the chemical industry, smelting, and power generation). Hydrogen consumption could replace fossil energy to achieve zero carbon emissions from the application side [25]. In the GTCC, through the transformation or development of burners, the proportion of hydrogen in natural gas might continuously increase, and finally, pure hydrogen could be utilized as a fuel. Most manufacturers have aimed to provide GTs that can burn pure hydrogen under all working conditions by developing DLE burners. However, it is currently challenging to achieve this aim without compromising costs and operating safety. When the above elements mature, the hydrogen-fired GT could become the backbone of the power energy structure due to its zero-carbon and low-NO_x emissions.

The concept of a hydrogen-fired combined cycle with water recovery is illustrated in Fig. 1. In this diagram, compressed air and hydrogen are mixed and burned in the CC to spin the turbine for power. Then, the exhaust gas enters the HRSG to heat the feed water to form steam to generate power. Finally, the exhaust gas is discharged into the WRC for water recycling. The recovered water compensates for the steam lost by the industrial heat supply. Any remaining water is used as other industrially consumed water in the power plant. The proposed combined cycle would be valuable for industrial operations, as it adopts a DLE burner to extend the equipment service life and reduce the use of industrial water.

3. Methodology

GTCCs with hydrogen and natural gas fuels have similarities in their compositions. Thus, the proposed concept in Section 2 was applied to an F-class natural-gas-fired power plant for thermodynamic simulations. The boundary conditions and component characteristics of this hydrogen-fired cycle were assumed to be the same as those of an actual natural-gas-fired power plant. In this section, the layout of hydrogen-fired combined cycles, the modeling formulas, and the performance and economic indices that can be used to evaluate this proposed cycle are presented.

3.1. Layout of hydrogen-fired combined cycles

The layout of a hydrogen-fired combined cycle without water recovery is depicted in Fig. 2(a) for comparison with the proposed concept. In the hydrogen-fired combined cycle, a single-shaft GT and an HRSG are integrated with a high-pressure turbine (HPT), an intermediate-pressure turbine (IPT), a low-pressure turbine (LPT), and a condenser in this cycle. Compressed air and hydrogen are burned at extremely high temperatures, causing the turbine blades to spin to generate power. The GT exhaust gas enters the HRSG to heat the feed water into steam. In the HRSG, the high-pressure and intermediate-pressure steam can be used as an industrial heat supply and for power generation. Specifically, the high-pressure steam passes through the HPT and is subsequently mixed with the intermediate-pressure steam to flow into the reheater and the IPT in turn. A similar process occurs in the LPT for power. Eventually, the steam is condensed into water to realize the Rankine cycle.

Recovering water from the exhaust gas is essential to the performance and economics of the combined cycle, because it can decrease the GT backpressure and compensate for the heat supply. In addition, the remaining recovered water has other industrial uses (e.g., hydrogen electrolysis), if needed. As shown in Fig. 2(b), the concept in Fig. 1 is implemented by installing water supplement devices at the end of the HRSG. Specifically, a WRC and an EGB are integrated with the hydrogen-fired combined cycle. The exhaust gas is introduced into the WRC to condense the water vapor in it. The condensed water is fed into the hydrogen-fired combined cycle to replenish the water supply. The EGB is used to exhaust the condensed exhaust water into the atmosphere.

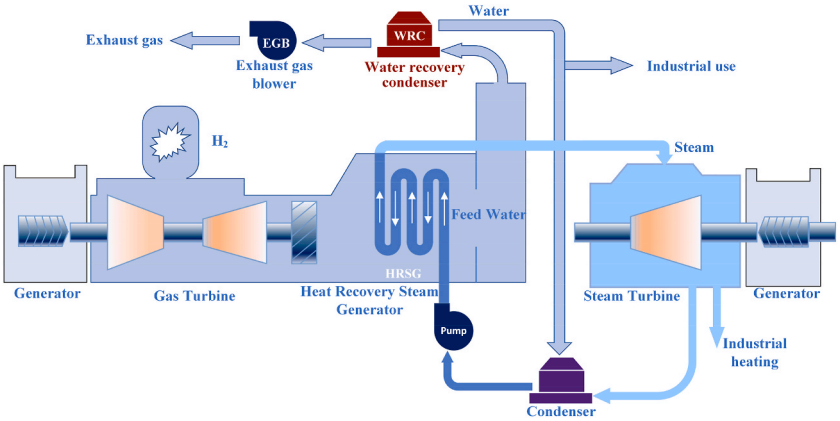

Fig. 1. Hydrogen-fired combined cycle with water recovery.

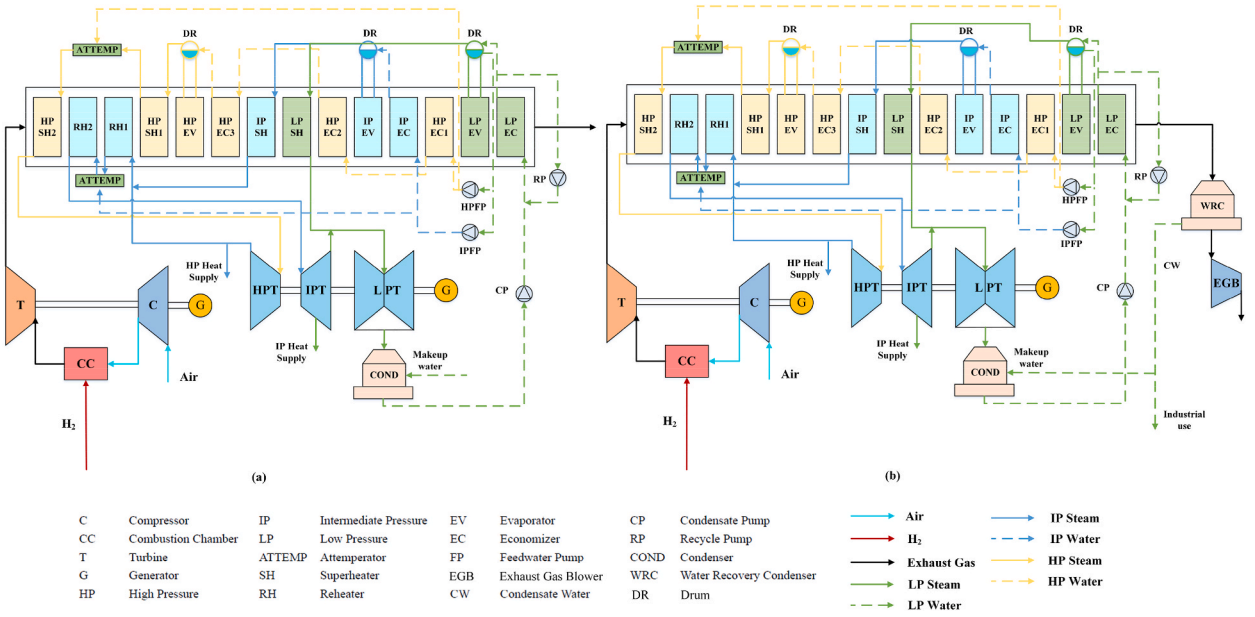

Fig. 2. Hydrogen-fired combined cycles (a) without water recovery and (b) with water recovery.

3.2. Modular modeling

The modeling formulas of the core components, including the compressor, CC, turbine, steam turbine, heat exchanger, drum, generator, pump, mixer, splitter, and WRC, are presented in this subsection. According to the modeling formulas, the thermodynamic model of the hydrogen-fired combined cycle with water recovery is established based on the operating data of an actual GTCC power plant in the IPSEPro software. Hundreds of equations need to be solved by iteration. In addition, variable working conditions are considered through the process of characteristic diagram interpolation.

Compressor. The compressor performance characteristics are usually given in the form of diagrams or curves. With the pressure ratio π_C and corrected speed n_C as independent variables, the corrected flow rate G_C and efficiency η_C can be expressed by the following functions:

$$G_C = f_1(\pi_C, n_C) \tag{1}$$

$$\eta_C = f_2(\pi_C, n_C) \tag{2}$$

The four characteristic variables are defined as follows:

$$G_C = G_1\sqrt{t_1}/p_1 \tag{3}$$

$$\pi_C = p_2/p_1 \tag{4}$$

$$n_C = n/\sqrt{t_1} \tag{5}$$

$$\eta_C = \Delta hs_C / (h_2 - h_1) \tag{6}$$

where G, t, p, h, and n are the mass flow rate, absolute temperature, absolute pressure, enthalpy, and rotation speed, respectively; Δhs_C is the isentropic enthalpy difference of the compression process; and subscripts "1" and "2" represent the compressor inlet and outlet, respectively.

The power P_C consumed by the compressor is

$$P_C = G_1 \times (h_2 - h_1) \tag{7}$$

Combustion chamber. The CC satisfies the following mass conservation equation:

$$G_2 + G_f = G_3 \tag{8}$$

where the subscript "f" represents the fuel injected into the CC, and subscript "3" refers to the CC outlet.

The standard enthalpy of formation is considered for energy conservation, as follows:

$$G_f = \frac{3600 C_p}{LHV \eta_f} G_C[(1+l)t_3 - t_2], \tag{9}$$

where C_p is the specific heat at constant pressure, LHV is the lower heating value of the fuel, η_f is the combustion efficiency, l is the air–fuel ratio, t_3 is the inlet temperature of the turbine, and t_2 is the outlet temperature of the compressor.

The total pressure recovery coefficient α is introduced into the CC to describe its pressure loss:

$$p_2 \times \alpha = p_3 \tag{10}$$

Turbine and steam turbine. Like the compressor, the turbine performance can also be described through four characteristic variables: the expansion ratio π_T, corrected speed n_T, corrected flow rate G_T, and efficiency η_T:

$$G_T = f_3(\pi_T, n_T) \tag{11}$$

$$\eta_t = f_4(\pi_T, n_T) \tag{12}$$

In Eqs. (11) and (12), the four variables are defined as follows:

$$G_T = G_3 \sqrt{t_3} / p_3 \tag{13}$$

$$\pi_T = p_3 / p_4 \tag{14}$$

$$n_T = n / \sqrt{t_3} \tag{15}$$

$$\eta_T = (h_3 - h_4) / \Delta hs_T \tag{16}$$

where the subscript "4" refers to the turbine outlet, and Δhs_T is the turbine isentropic enthalpy difference.

The power produced by the turbine P_T is calculated as follows:

$$P_T = G_3 \times (h_3 - h_4) \tag{17}$$

Heat exchanger. The heat exchanger transfers heat from the hot fluid to the cold fluid. Since the two fluids do not mix, the inlet and outlet flows of the two fluids are equal. Then, energy conservation is expressed as follows:

$$Q = G_{hf} \times \left(h'_{hf} - h''_{hf}\right) = G_{cf} \times \left(h''_{cf} - h'_{cf}\right) \tag{18}$$

where Q is the heat exchange amount, the subscripts "*hf*" and "cf" represent the hot fluid and cold fluid, respectively, and the superscripts ' and " refer to the fluid inlet and outlet, respectively. Since it is a countercurrent heat exchanger, the logarithmic mean temperature difference LnD is expressed as

$$LnD = (\Delta t'' - \Delta t') / ln(\Delta t'' / \Delta t') \tag{19}$$

$$\Delta t' = t'_{hf} - t''_{cf} \tag{20}$$

$$\Delta t'' = t''_{hf} - t'_{cf} \tag{21}$$

where Δt is the temperature difference.

As a result, the heat exchange amount Q can also be calculated based on the heat transfer coefficient k and heat transfer area A:

$$Q = k \times A \times LnD \tag{22}$$

Drum. Assuming that the drum is always in a steady state, its conservation equations are as follows:

$$G_{EC} + G'_{EV} = G_{SH} + G''_{EV} \tag{23}$$

$$G_{EC} \bullet h_{EC} + G'_{EV} \bullet h'_{EV} = G_{SH} \bullet h_{SH} + G''_{EV} \bullet h''_{EV} \tag{24}$$

where the subscripts "*EC*," "*EV*," and "*SH*" denote the economizer, evaporator, and superheater, respectively.

The temperature difference at the approach point dt_{app} is defined as the difference between the economizer outlet temperature t_{EC} and the saturated steam temperature t_{SA} under the saturated pressure:

$$dt_{app} = t_{SA} - t_{EC} \tag{25}$$

Generator. The power generation capacity of a generator is calculated by its power generation efficiency η_{el} and mechanical efficiency η_m:

$$P_{gen} = P_{shaft} \bullet \eta_{el} \bullet \eta_m \tag{26}$$

where P_{gen} and P_{shaft} are the electrical power produced by the generator and the shaft power of the generator, respectively.

Pump. The process of pumping the fluid is described as

$$P_{shaft} \bullet \eta_m = G_p^{'} \bullet \left(h_p^{''} - h_p^{'}\right) \tag{27}$$

where the subscript "*p*" refers to the pump. Since the whole process is non-isentropic, its isentropic efficiency η_p is introduced as follows:

$$\eta_p = \Delta hs_p \Big/ \left(h_p^{''} - h_p^{'}\right) \tag{28}$$

Mixer. The mixer mixes two different fluids, satisfying the following mass and energy balances:

$$G_{mix1} + G_{mix2} = G_{mix3} \tag{29}$$

$$G_{mix1} \bullet h_{mix1} + G_{mix2} \bullet h_{mix2} = G_{mix3} \bullet h_{mix3} \tag{30}$$

where the subscripts "*mix1*," "*mix2*," and "*mix3*" refer to the first inlet fluid, second inlet fluid, and outlet fluid, respectively.

Splitter. The splitter splits one fluid into two fluids:

$$G_{spl3} = G_{spl1} + G_{spl2} \tag{31}$$

$$h_{spl3} = h_{spl1} = h_{spl2} \tag{32}$$

where the subscripts "*spl1*," "*spl2*," and "*spl3*" denote the first outlet fluid, second outlet fluid, and inlet fluid, respectively.

Water recovery condenser. The working principles of a condenser and a heat exchanger are similar; so, the condenser's heat transfer formulas are omitted in this section. The exhaust gas can hold different moisture contents at different temperatures, and the maximum moisture content decreases as its temperature drops. Fig. 3 shows the water recovery process.

In state 1 (i.e., unsaturated state), no recovered water is produced when changing from state 1 to state A, and thus, the moisture content *d* does not change. When the exhaust gas reaches state A (i.e., saturated state), its relative humidity φ reaches 100%. The saturated temperature at state A is also known as the dew point temperature. As the temperature continuously drops, the thermal state changes from state A to state 2. During this process, φ has been maintained at 100%, while the steam in the exhaust gas is still saturated. The liquid water begins to condense, and thus *d* continues to decrease. The WRC extracts the steam from the exhaust gas, which is converted into water through cooling. The mass conservation is as follows:

$$G_{WRC}^{'} = G_{WRC}^{''} + G_{CW} \tag{33}$$

where the subscripts "*WRC*" and "*CW*" represent the water recovery condenser and the condensed water, respectively, and the superscripts ' and '' refer to the inlet and outlet, respectively.

The moisture content *d* (kg/kg DA) is defined as

$$d = 0.622 \times p_v / (p_a - p_v) \tag{34}$$

where p_v and p_a are the water vapor partial pressure and the exhaust gas pressure, respectively. Since the exhaust gas at the WRC outlet

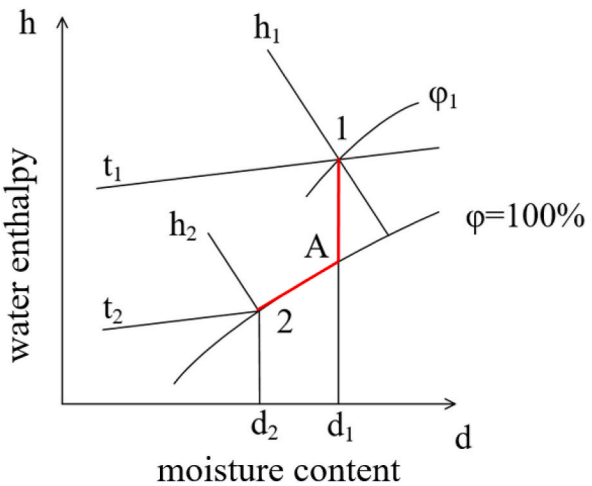

Fig. 3. Schematic diagram of the water recovery process.

is saturated, its outlet temperature is equal to the saturated temperature.

3.3. Evaluation indices

3.3.1. Performance indices

To analyze the GTCC performance, the performance parameters of the components were selected as the comparison indices, such as the fuel flow rate G_f and the GT thermal efficiency η_{GT}. From an overall perspective, the performance based on the total output power P_{GTCC} and the net thermal efficiency η_{GTCC} is evaluated [26,27]. P_{GTCC} is defined as

$$P_{GTCC} = P_{GT} + P_{ST} \tag{35}$$

where P_{GT} is the power generated by the GT, and P_{ST} is the power generated by the steam turbine.

LHV is the lower heating value of the corresponding fuel. P_{EGB} is the power consumed by the EGB when the hydrogen-fired combined cycle has the water recovery system. η_{GT} and η_{GTCC} are defined as follows:

$$\eta_{GT} = \frac{P_{GT}}{G_f * LHV} \tag{36}$$

$$\eta_{GTCC} = \frac{P_{GTCC-P_{EGB}}}{G_f * LHV} \tag{37}$$

Moreover, natural gas and hydrogen are uniformly converted into standard coal to measure the heat consumption. The definition of the standard coal equivalent G_{SC} is

$$G_{SC} = \frac{G_f * LHV}{LHV_{SC}} \tag{38}$$

where LHV_{SC} is the net calorific value of standard coal, which equals 29,307.6 kJ/kg [28].

3.3.2. Economic indices

The levelized cost of electricity (LCOE, $/MWh) can evaluate the economic feasibility of energy projects quantitatively. It is the minimum electricity sale price required for the power plant to break even [29]. The common definition of the LCOE in one specific year, which is applied in this paper, is as follows [30]:

$$LCOE = I + F + Em + M = \frac{I_{total}/OT + (Em_t + F_t + M_t)}{ELE_t} \tag{39}$$

where the LCOE is divided into four main parts: the investment cost I, the fuel cost F, the emission cost Em, and the maintenance cost M. As a one-time cost, the investment cost should be averaged over the total investment cost I_{total} within the system operating time OT. The other kinds of costs are defined as annual costs for the current year, which are denoted by the subscript t. Fuel cost includes the cost of buying and transporting fuel. Emission cost indicates the cost of exhaust gas emitted. Maintenance cost includes operation maintenance, insurance, and overhead. For simplicity, some items are disregarded, such as potential revenue and asset depreciation [31]. ELE_t represents the electricity generated in 1 year. In addition to the LCOE under the full working conditions, the LCOEs under variable working conditions are also studied in this paper, which may be increasingly common in the electricity sector [31].

For a real scenario, Eq. (39) can be refined to describe the economic indices of the natural-gas-fired combined cycle and hydrogen-fired combined cycle. For a natural-gas-fired combined cycle, the LCOE in year y can be defined specifically as follows:

$$LCOE_{NG,y} = \frac{c_{ivm}/OT + \left(c_y + c_{trans,d,y}\right) * G_f + G_{ccs} * Pr_{ccs,y} + G_{ue} * Pr_{co_2,y} + c_{mnt}}{ELE_{GTCC}} \tag{40}$$

where c_{ivm} is the equipment investment cost, c_y is the fuel cost in year y, $c_{trans,d,y}$ is the transportation cost via a specific transport route for some distance d in year y, G_f is the fuel consumption, G_{ccs} represents the captured CO_2 emissions, $Pr_{ccs,y}$ is the cost of transporting and storing CO_2 in year y, G_{ue} represents the uncaptured CO_2 emissions, $Pr_{co_2,y}$ is the CO_2 price in year y, c_{mnt} is the maintenance cost, and ELE_{GTCC} is the electricity produced by the GTCC.

For the hydrogen-fired combined cycle, the LCOE can be refined as follows:

Table 1
Costs for economic evaluation.

Item	2020	2030	2050	References
c_y and $c_{trans,d,y}$ of hydrogen ($/kg)	4.418	2.425	1.55	[32]
c_y and $c_{trans,d,y}$ of natural gas ($/kg)	1.188	1.307	1.581	[33,34]
$Pr_{ccs,y}$ ($/kg)	0.0499	0.065	0.084	[35]
$Pr_{co_2,y}$ ($/kg)	0.0255	0.0912	0.146	[36]
Carbon capture rate	80%	90%	95%	[37]

$$LCOE_{H_2,y} = \frac{c_{ivm}/OT + \left(c_y + c_{trans,d,y}\right) * G_f + c_{mnt}}{ELE_{GTCC}} \quad (41)$$

where c_{ivm} is the equipment investment cost, including modifying the equipment or adding a water recovery system, c_y is the fuel cost in year y, $c_{trans,d,y}$ is the transportation cost via a specific transport route for some distance d in year y, G_f is the fuel consumption, c_{mnt} is the maintenance cost, and ELE_{GTCC} is the electricity produced by the GTCC.

Various costs related to the economic evaluation involved in forecasting the LCOE of the natural-gas-fired combined cycle and hydrogen-fired combined cycle are listed in Table 1. It should be noted that inflation and exchange rate changes were not considered. Natural gas prices are volatile; however, since factors such as climate and crude oil extraction are unknown, the price was assumed to increase by 10% per decade. In addition, $Pr_{ccs,y}$ was simplified as the unrestricted cost, including all forms of storage and the transport costs over 100 km. Both captured CO_2 prices and uncaptured CO_2 prices increase over time. Although fossil-based hydrogen production is currently more cost-effective than renewable-energy-based hydrogen production, some studies have suggested that the latter will continue to decline and become cost-competitive with fossil-based hydrogen [38,39]. Compared with the natural-gas-fired combined cycle, there are additional equipment costs of the hydrogen-fired combined cycle caused by the WRC. Based on the costs of the WRC, the investment cost of the hydrogen-fired combined cycle with water recovery evenly distributed to each service year was assumed to be increased by $717.36 [40]. The maintenance costs were assumed to be 3% of the total cost.

4. Results and discussion

The natural-gas-fired combined cycle was modeled first, and the results were used as the reference case for this study. Then, the hydrogen-fired combined cycles with and without water recovery were also modeled for comparison. The physical properties in the models were set for 12 components (Ar, C_2H_6, C_3H_8, CH_4, CO, CO_2, H_2, H_2O, H_2S, N_2, O_2, and SO_2). The mass fractions (kg/kg) of air, natural gas, and hydrogen are listed in Table 2. The effect of humid air on the physical properties was taken into consideration for hydrogen combustion [41]. Based on the compositions of the natural gas and hydrogen streams, their net calorific values were obtained as 48,142 and 120,000 kJ/kg, respectively [42].

The model inputs have two categories: component characteristic parameters (e.g., compressor efficiency and CC pressure loss) and boundary conditions (e.g., ambient temperature and pressure). The main inputs of the three models were the same under full and variable working conditions, as shown in Table 3. The inputs were all selected from actual operating data of a real F-class gas turbine combined cycle power plant located in Kunshan, China. The inputs included the compressor inlet pressure p_1, compressor inlet temperature t_1, compressor efficiency η_C, turbine efficiency η_T, turbine inlet temperature t_3, GT output power P_{GT}, HPT efficiency η_{HPT}, IPT efficiency η_{IPT}, LPT efficiency η_{LPT}, and steam turbine vacuum p_{ES}. Full working conditions and six variable working conditions were captured from the sensor data (April 2019–August 2020) of this selected gas turbine power plant. The full working conditions were based on a 100% load, and the variable working conditions were based on loads of 50%, 60%, 70%, 80%, 90%, and 110%. The boundary conditions (p_1, t_1, P_{GT}, p_{ES}) were obtained directly from the sensor data. The component characteristic parameters (η_C, η_T, t_3, η_{HPT}, η_{IPT}, η_{LPT}) were obtained from the simulation results of the combined cycle models. The design efficiencies are set according to the design parameters. The efficiencies of the compressor and turbine under variable working conditions are obtained by the component characteristic curves according to the corresponding parameters (π_C, n_C for the compressor and π_T, n_T for the turbine) [43,44]. The corresponding parameters are calculated based on the sensor data. In addition, the efficiency of combustion under variable working conditions is affected by some factors such as the fuel/air ratio and the inlet pressure [45]. It is set based on the general empirical formula.

The required sensor data were input into the combined cycle models first to calculate characteristic parameters. Then, these characteristic parameters were set as model inputs for the comparison of different combined cycles.

After modeling, the model accuracy for the natural gas and hydrogen simulations is discussed in Section 4.1. A comparison of the hydrogen-fired cycle without water recovery and the natural-gas-fired cycle is presented in Section 4.2. Moreover, the performance and economics are analyzed by comparing the hydrogen-fired cycles with and without water recovery in Section 4.3.

Table 2
Mass fractions of air, natural gas, and hydrogen.

Symbols	Meaning	Air	Hydrogen	Natural Gas
Ar	Argon	0.01273	0	0
C_2H_6	Ethane	0	0	0.06697
C_3H_8	Propane	0	0	0.01238
CH_4	Methane	0	0	0.88695
CO	Carbon monoxide	0	0	0
CO_2	Carbon dioxide	0.00111	0	0.01485
H_2	Hydrogen	0	1	0
H_2O	Water	0.0083	0	0
H_2S	Hydrogen sulfide	0	0	0
N_2	Nitrogen	0.74845	0	0.01885
O_2	Oxygen	0.22941	0	0
SO_2	Sulfur dioxide	0	0	0

Table 3
Main inputs of the compared models.

Parameters	Unit	110%	100%	90%	80%	70%	60%	50%
p_1	kPa	102.40	101.54	100.04	100.10	101.70	102.20	101.60
t_1	K	276.24	286.921	292.87	290.14	290.93	290.77	286.37
η_C	%	89.04	91.23	90.14	89.92	89.62	88.69	85.66
η_T	%	86.65	87.44	87.69	86.01	85.53	84.99	84.10
t_3	K	1589.95	1597.35	1580.15	1549.75	1522.25	1493.65	1461.05
P_{GT}	MW	310.91	296.29	270.48	240.32	210.80	181.53	151.96
η_{HPT}	%	78.23	77.75	78.16	78.42	89.06	95.83	92.46
η_{IPT}	%	88.57	81.90	85.96	82.21	74.65	83.12	86.08
η_{LPT}	%	88.07	89.23	92.95	85.31	88.43	85.59	85.56
p_{ES}	kPa	5.83	6.72	7.16	8.13	6.12	6.18	6.17

4.1. Model accuracy

The model accuracy of the natural-gas-fired combined cycle was verified first based on the operating data of the F-class power plant. The errors between the simulation results and the actual measurements were calculated. The selected measurements included the exhaust gas flow, superheated steam flow, and steam turbine power. The exhaust gas temperature at the outlet of the low-pressure economizer had a maximum error of 0.546%. The other errors were less than 0.02%. The model accuracy of the natural-gas-fired combined cycle was high enough for subsequent analysis.

Then, the model accuracy of the hydrogen-fired combined cycle was validated based on the first hydrogen power plant in the world and the simulation results in another reference paper. Because the hydrogen-fired combined cycle is still in the research phase, no mature F-class power plant is available to use pure hydrogen as a fuel. For the model using hydrogen, ENEL's Fusina Hydrogen project was selected for comparison. The Fusina power plant was used to verify the correct operation of the gas turbine with pure hydrogen as a fuel and acquire know-how for hydrogen combustion, safety aspects, and control technologies for the gas cycles. It had a measured GT efficiency of 31.1% for almost 12 MW of delivered power [24]. According to the hydrogen model in this paper, the GT efficiency was 39.85%, which was higher than the measured efficiency reported above. A primary reason for this is that the hydrogen-fired combined cycle was applied to an F-class power plant, which delivered about 400 MW of power more than 12 MW. In Ditaranto's research [11], high-hydrogen-content fuels were also applied to an F-class power plant, and the GT efficiency was about 39.5%, which was very close to the result obtained in this paper. Therefore, the model accuracy for hydrogen was validated.

4.2. Comparative case study of hydrogen-fired combined cycle without water recovery and natural-gas-fired combined cycle

In this subsection, the hydrogen-fired combined cycle without water recovery is compared to the natural-gas-fired combined cycle in terms of performance and economics.

4.2.1. Full working conditions

Table 4 shows sharp drops in the fuel mass flow rate G_f and exhaust gas flow rate G_{EG} for the hydrogen fuel compared to those of natural gas. Moreover, the high calorific value of hydrogen led to a minor increase in the steam turbine power P_{ST} despite the decrease in G_{EG}. However, the η_{GT} and η_{GTCC} of the hydrogen-fired combined cycle without water recovery increased by 0.72% and 1.35%, respectively. The standard coal equivalent G_{SC} of hydrogen was lower than that of natural gas. The results revealed that the hydrogen-fired combined cycle without water recovery improved the equipment performance over the natural-gas-fired combined cycle.

The LCOE indices of the two combined cycles in 2020, 2030, and 2050 were calculated, as shown in Fig. 4. Compared with the natural-gas-fired combined cycle, the LCOE of the hydrogen-fired combined cycle did not include the emission cost. The LCOE of the hydrogen-fired cycle dropped sharply owing to the vigorous development of hydrogen energy within a few decades, which will bring high economic benefits.

Pure hydrogen combustion has products rich in water vapor. A small amount of CO_2 included in the exhaust gas using hydrogen fuel originated from the air sucked into the compressor. As shown in Table 5, the mass fraction of H_2O was 0.096425 kg/kg. According to the psychrometric chart, the moisture content equaled 0.107 kg/kg, and the water vapor partial pressure was 14.61 kPa when it was saturated under the standard ambient pressure (i.e., 101.325 kPa). Hence, this exhaust gas at the HRSG outlet had the full potential for water to be extracted for recycling. In addition, the exhaust gas using natural gas fuel contained abundant CO_2. CO_2 emissions

Table 4
Comparison of results for natural gas and hydrogen fuels under full working conditions.

Parameters	Unit	Natural Gas	Hydrogen
G_f	kg·s^{-1}	15.74	6.20
t_4	K	921.51	922.66
G_{EG}	kg·s^{-1}	655.00	628.00
P_{ST}	MW	107.36	110.12
η_{GT}	%	39.10	39.82
η_{GTCC}	%	53.27	54.62
G_{SC}	kg·s^{-1}	25.85	25.38

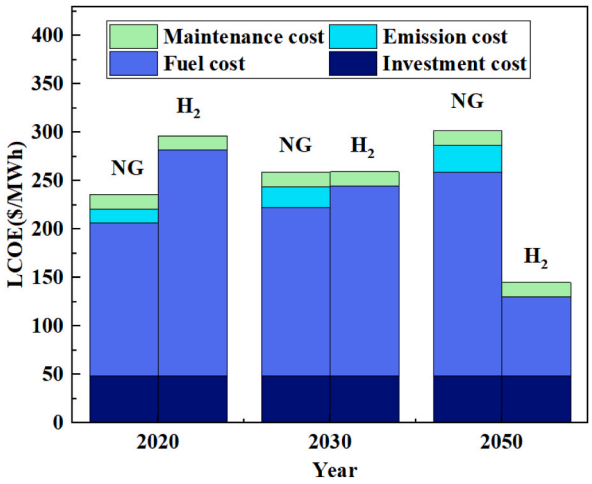

Fig. 4. Levelized cost of electricity (LCOE) of natural-gas-fired combined cycle and hydrogen-fired combined cycle under full working conditions.

Table 5
Mass fractions of the exhaust gas using hydrogen or natural gas as a fuel.

Symbol	Meaning	Hydrogen combustion exhaust	Natural gas combustion exhaust
Ar	Argon	0.012604	0.012424
C_2H_6	Ethane	0	0
C_3H_8	Propane	0	0
CH_4	Methane	0	0
CO	Carbon monoxide	0	0
CO_2	Carbon dioxide	0.001099	0.065521
H_2	Hydrogen	0	0
H_2O	Water	0.096425	0.059356
H_2S	Hydrogen sulfide	0	0
N_2	Nitrogen	0.74106	0.73091
O_2	Oxygen	0.14881	0.13178
SO_2	Sulfur dioxide	0	0

aggravated the greenhouse effect, whereas hydrogen combustion produced only water without environmental pollution hazards.

4.2.2. *Variable working conditions*

The standard coal equivalent is a well-known criterion for performance evaluation. The fuel mass flow rates of the two kinds of cycles continuously decreased as the GTCC loads declined. The upper black and lower red dots in Fig. 5(a) indicated that natural gas emitted more exhaust gas than hydrogen. The hydrogen-fired GT always had a higher efficiency than the natural-gas-fired GT under the same working conditions due to its high calorific value in Fig. 5(b). The efficiency variations of two cycles with the loads were investigated to further assess the performance. As shown in Fig. 5(c), the GTCC efficiency for the 70% load was the highest of all the loads because it had the lowest heat supply requirement. The superior performance of the hydrogen cycle, to some extent, could be validated accurately based on the GT and GTCC efficiencies considering the heat supply. The specific values are listed in Appendix A.

Fig. 6 shows the variation tendencies of the LCOE indices of the natural-gas and hydrogen under variable working conditions in different years. The relative deviations of the LCOEs for these two kinds of combined cycles are also illustrated in Fig. 6 to demonstrate the economic improvement of the hydrogen-fired combined cycle. The relative deviations of LCOEs are the ratio of the absolute deviations (LCOE of the hydrogen-fired combined cycle minus LCOE of the natural-gas-fired combined cycle) to the LCOE of the natural-gas-fired combined cycle. The LCOE indices generally increased as the load decreased. The most probable reasons for the LCOE fluctuation were the different heat supplies and gas turbine powers over the load range. According to the reference data in 2020, hydrogen had a higher LCOE than natural gas because of the lack of industrial experience. The LCOE of the hydrogen-fired combined cycle gradually decreased with the decrease in the cost of hydrogen production. Meanwhile, the LCOE of the natural-gas-fired combined cycle increased with increasing cost of emissions. Therefore, the LCOEs of both combined cycles will be very close in 2030, as shown in Fig. 6(b). The hydrogen-fired combined cycle will become more competitive as the hydrogen production cost decreases in 2050, as shown in Fig. 6(c). In 2050, the LCOE of the hydrogen-fired combined cycle decreased by 52% compared to that of the natural-gas-fired combined cycle under the 100% load condition.

4.3. *Comparative case study of hydrogen-fired combined cycle with/without water recovery*

Hydrogen combustion results in a great deal of water vapor, as discussed in Section 2. If the exhaust gas were directly discharged

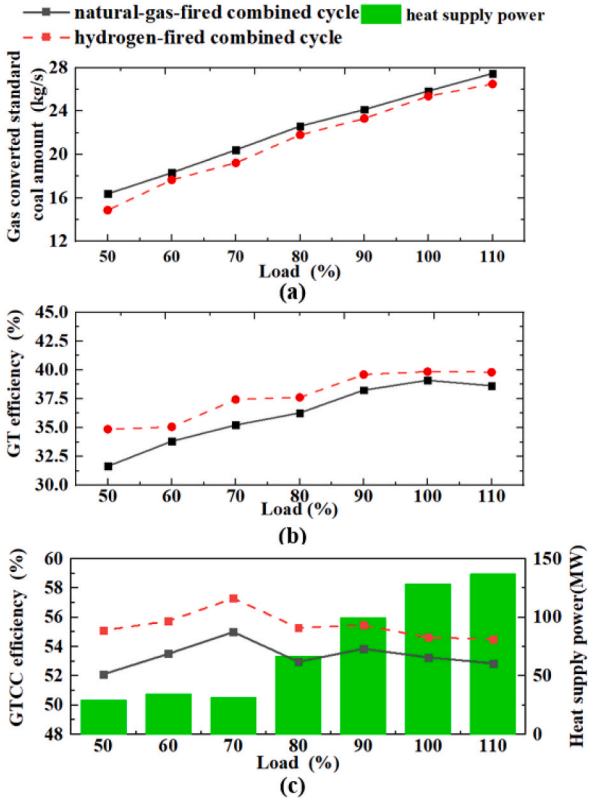

Fig. 5. Changes in (a) standard coal equivalent, (b) gas turbine (GT) efficiency, and (c) gas turbine combined cycle (GTCC) efficiency under variable working conditions.

into the atmosphere, it would cause considerable losses. Water recovery is an effective method for conserving water resources and compensating for the heat supply in the steam turbine. The performances and economics of the hydrogen-fired combined cycle with and without water recovery are compared in this section. In the combined cycle with water recovery, some inputs of the new components should be set, including the HRSG outlet pressure, WRC circulating water temperature, and EGB efficiency.

Heat recovery steam generator (HRSG) outlet pressure. During the condensation process, the specific volume of the steam in the exhaust gas declined dramatically. Thus, the water vapor partial pressure dropped rapidly, and the exhaust gas formed a vacuum inside the condenser. When establishing the GTCC model, it is necessary to set the vacuum degree of the condenser. Since the partial pressure of water vapor calculated at the total pressure of 101.4 kPa was about 14.61 kPa, the partial pressure sum of the remaining dry air components was 86.79 kPa. Considering that it was difficult for the condenser to condense all the water vapor in the air, the air at the outlet of the condenser still contained some water vapor. Thus, there was a certain partial pressure of water vapor; so, the pressure there was higher than the limit pressure of 86.79 kPa. The exhaust gas at the condenser outlet was saturated and retained a small amount of water vapor.

Water recovery condenser (WRC) circulating water temperature. The cooling circulating water of the WRC was used to exchange heat with the exhaust gas at the HRSG outlet. In this case, the amount was set to be the same as that of the circulating water of the condenser after the steam turbines.

Exhaust gas blower (EGB) efficiency. It was difficult for the exhaust gas to be discharged without any power because of its negative pressure relative to atmospheric pressure. Consequently, the left exhaust gas was extracted by the EGB when the water vapor in the WRC was condensed to liquid water, and then, the exhaust gas was continuously discharged into the atmosphere. In this case, the EGB efficiency was set to 0.8 according to a previous publication [46].

4.3.1. Full working conditions

As shown in Table 6, the G_f values of the combined cycle with and without water recovery were 6.20 and 6.04 kg/s, respectively. The cycle with water recovery had slightly lower G_f and G_{EG} values compared to the cycle without water recovery. In addition, t_4 dropped by almost 10 K. Hence, the amount of steam produced by the HRSG was also lower, and P_{ST} declined from 110.12 to 103.72 MW.

From an efficiency perspective, the η_{GT} and η_{GTCC} values of the cycle with water recovery were 1.06% and 0.57% higher than those of the cycle without water recovery, respectively. Compared to the cycle without water recovery, the G_{SC} value of the cycle with water recovery decreased by 0.65 kg/s. Overall, the combined cycle with water recovery had a higher efficiency due to the low pressure at the

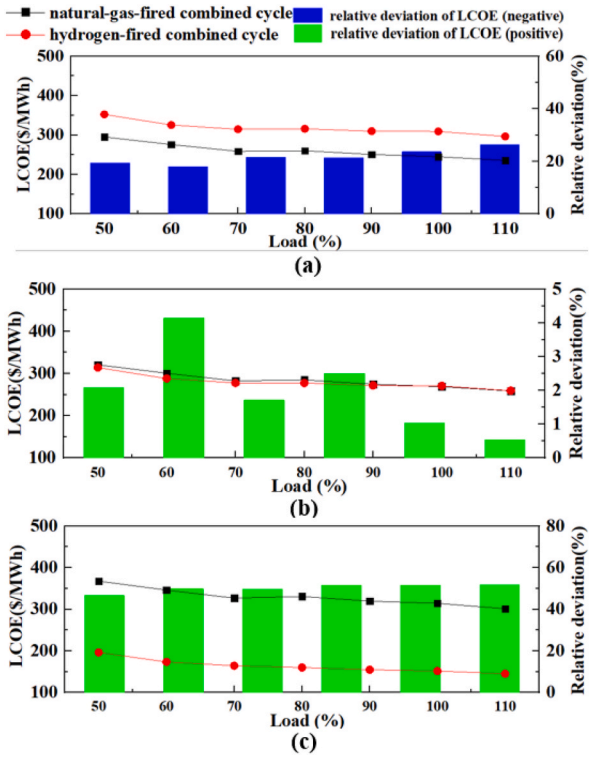

Fig. 6. Changes of levelized cost of electricity (LCOE) in variable working conditions in (a) 2020, (b) 2030, and (c) 2050.

Table 6
Result comparison of the combined cycles with/without water recovery.

Parameters	Unit	Without water recovery	With water recovery
G_f	kg·s^{-1}	6.20	6.04
t_4	K	922.66	912.71
G_{EG}	kg·s^{-1}	628.00	612.20
P_{ST}	MW	110.12	103.72
G_{CW}	kg·s^{-1}	/	50.34
P_{EGB}	MW	/	3.91
η_{GT}	%	39.82	40.88
η_{GTCC}	%	54.62	55.19
G_{SC}	kg·s^{-1}	25.38	24.73

HRSG outlet.

As shown in Fig. 7, the LCOE indices of the two cycles were calculated. In 2020, the LCOE indices of these two cycles were 293.32 and 296.41 $/MWh. The combined cycle with water recovery had a slightly higher investment cost due to the water recovery system. The fuel cost of the combined cycle with water recovery was lower than that of the combined cycle without water recovery.

4.3.2. Variable working conditions

The hydrogen-fired combined cycle with water recovery consumed less hydrogen per second under variable working conditions. A primary reason for the high performance was that the water recovery technology cut down the GT outlet pressure. As shown in Fig. 8 (b), the GT efficiency of the hydrogen-fired combined cycle with water recovery dropped by about 5.6%, and the GTCC efficiency fluctuated up and down due to the different amounts of heat supplied. The GTCC supplied more heat under high-load conditions, which led to low GTCC efficiencies for 80%, 90%, 100%, and 110% loads, as shown in Fig. 8(c). The cycle with water recovery always had a slightly higher efficiency and a lower standard coal equivalent compared to the cycle without water recovery.

Fig. 9 shows the comparison of the LCOE indices between the hydrogen-fired combined cycle with and without water recovery. The relative deviations are also shown in Fig. 9 to demonstrate the improvement in economy due to water recovery. The relative deviations of LCOEs are the ratio of the absolute deviations (LCOE of the hydrogen-fired combined cycle with water recovery minus LCOE of the hydrogen-fired combined cycle without water recovery) to the LCOE of the hydrogen-fired combined cycle without water recovery. The trend of the LCOE variation with the load was the same. Under a 100% load, the LCOE for the hydrogen-fired combined cycle with the water recovery cycle represented a better economic performance than that of the hydrogen-fired combined cycle without the water

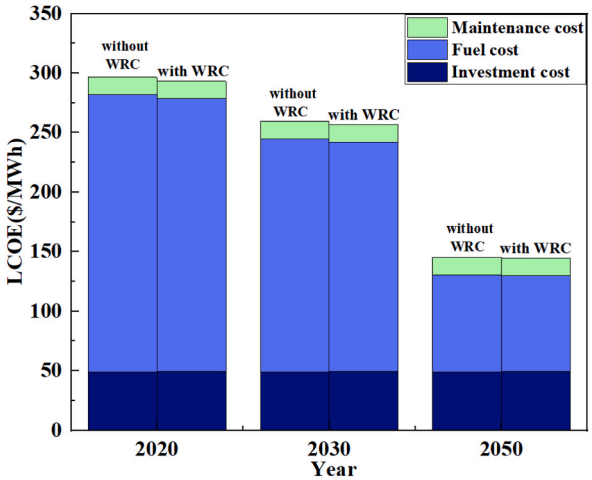

Fig. 7. Levelized cost of electricity (LCOE) of the hydrogen-fired combined cycle with and without water recovery under variable working conditions.

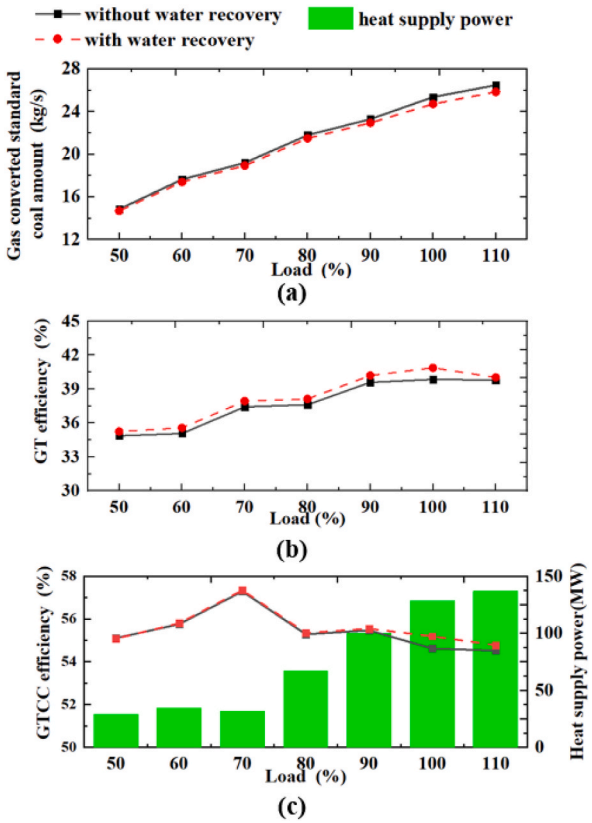

Fig. 8. Changes in (a) standard coal equivalent, (b) GT efficiency, and (c) GTCC efficiency under variable working conditions.

recovery cycle.

In addition, in this comparative case, the mass flow rate of the condensed water decreased from 50.34 to 29.83 kg/s as the load changed from 100% to 50%. A large amount of water was condensed from the exhaust gas to compensate for the loss of the steam turbine system due to external heat extraction.

5. Conclusions

Hydrogen development is an effective way to alleviate global climate change and energy shortages. A hydrogen-fired combined cycle with water recovery that integrated hydrogen power generation with industrial water recycling was proposed in this paper. The

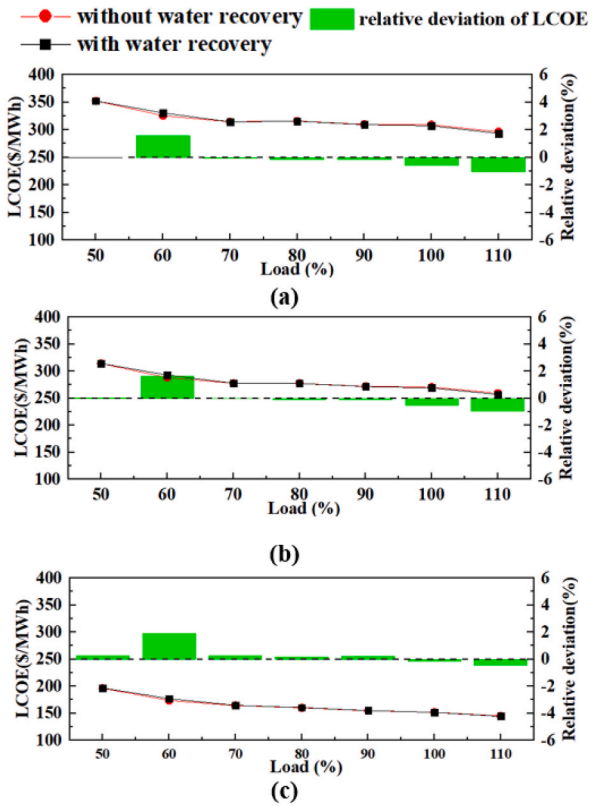

Fig. 9. Changes in LCOE indices of the hydrogen-fired combined cycle with and without water recovery under variable working conditions in (a) 2020, (b) 2030, and (c) 2050.

novelty of this work is that water recycling was incorporated into the concept of this paper, which decreased the loss of industrial water and reduced the environmental impact. This concept was applied to an F-class combined cycle power plant. Comparative studies of a hydrogen-fired combined cycle with/without water recovery and a natural-gas-fired combined cycle were conducted to analyze the performance and economics of the proposed combined cycle. The main findings of this study can be summarized as follows.

1) The model accuracy of the natural-gas-fired combined cycle was verified first based on the operating data of the F-class power plant. Then, the model accuracy of the hydrogen-fired combined cycle was validated based on the first hydrogen power plant in the world and the simulation results presented in a previous study.
2) The amount of recovered water for a 100% load was 50.34 kg/s, which could be applied to industrial heat supply compensation and other industrial uses. The gas turbine efficiency and combined cycle efficiency increased by 1.06% and 0.57%, respectively, when the water recovery system was added. Therefore, it was concluded that adding an exhaust gas condenser at the HRSG outlet could recover water, as well as lessen the gas turbine backpressure and improve gas turbine performance.
3) In addition, an economic comparison of the three cycles was conducted. The hydrogen-fired combined cycle with water recovery had the lowest levelized cost of energy. According to the economic analysis results, the LCOE of the hydrogen-fired combined cycle without water recovery would be 52% lower than that of the natural-gas-fired combined cycle in 2050. The LCOE could be decreased by 0.22% by introducing water recovery. The economic performance suggested that the hydrogen-fired combined cycle could become competitive in the long term if its large-scale deployment reduces fuel costs.

The hydrogen-fired GT market may develop to achieve low emissions, rapid responses, and high efficiencies within a few decades. By that time, a concept like the hydrogen-fired combined cycle with water recovery could be applied to increase the total power plant efficiency and provide valuable support to reduce operational costs, conserve water resources, and protect the environment.

Author statement

Tingting Wei: Conceptualization, Writing – original draft, Writing – review & editing.
Zhenchao Hu: Visualization, Writing – review & editing.
Xingyu Tang: Software, Writing –original draft.
Huisheng Zhang: Supervision, Project administration, Funding acquisition.

Declaration of competing interest

The authors declare that they have no known competing financial interests or personal relationships that could have appeared to influence the work reported in this paper.

Data availability

Data will be made available on request.

Acknowledgments

This work was supported by the National Natural Science Foundation of China [grant number 51876116], the National Fundamental Research Project [grant numbers JCKY2017208A001, JCKY2019204B009, JCKY2020208B036, JCKY2021209B016, MKF20200020], and the Industry-University-Research Cooperation Project of AECC [grant number HFZL2019CXY028].

Appendix A. Supplementary data

Supplementary data to this article can be found online at https://doi.org/10.1016/j.csite.2023.102863.

References

[1] R.S. El-Emam, I. Khamis, Advances in nuclear hydrogen production: results from an IAEA international collaborative research project, Int. J. Hydrogen Energy 44 (35) (2019) 19080–19088, https://doi.org/10.1016/j.ijhydene.2018.04.012.
[2] H. Pollitt, Analysis: going carbon neutral by 2060 'will make China richer, Carbon Br 24 (2020). https://www.carbonbrief.org/analysis-going-carbon-neutral-by-2060-will-make-china-richer.
[3] R. Pavri, G.D. Moore, Gas Turbine Emissions and Control, vol. 1, Atlanta GE Energy Serv, 2001, pp. 1–20. https://www.eplptx.com/wp-content/uploads/2020/05/Gas-Turbine-Emissions-and-Control.pdf.
[4] Z. Huang, J. Wang, E. Hu, C. Tang, Y. Zhang, Progress in hydrogen enriched hydrocarbons combustion and engine applications, Front. Energy 8 (2014) 73–80, https://doi.org/10.1007/s11708-013-0287-1.
[5] M.R. Vanco, Thermodynamic and Turbine Characteristics of Hydrogen-Fueled Open-Cycle Auxiliary Space Power Systems, National Aeronautics and Space Administration, 1967.
[6] C. Forsberg, An air-brayton nuclear-hydrogen combined-cycle peak-and baseload electric plant, ASME International Mechanical Engineering Congress and Exposition 43009 (2007), https://doi.org/10.1115/IMECE200743907.
[7] H. Jericha, V. Hacker, W. Sanz, G. Zotter, Thermal steam power plant fired by hydrogen and oxygen in stoichiometric ratio, using fuel cells and gas turbine cycle components, Turbo Expo: Power for Land, Sea, and Air 43987 (2010), https://doi.org/10.1115/GT2010-22282.
[8] F. Toja-Silva, A. Rovira, A first and second thermodynamics law analysis of a hydrogen-fueled microgas turbine for combined heat and power generation, J. Eng. Gas Turbines Power 136 (2014) 2, https://doi.org/10.1115/1.4025321.
[9] W. Sanz, M. Braun, H. Jericha, M.F. Platzer, Adapting the zero-emission Graz Cycle for hydrogen combustion and investigation of its part load behavior, Int. J. Hydrogen Energy 43 (11) (2018) 5737–5746, https://doi.org/10.1016/j.ijhydene.2018.01.162.
[10] A. Arsalis, Thermodynamic modeling and parametric study of a small-scale natural gas/hydrogen-fueled gas turbine system for decentralized applications, Sustain. Energy Technol. Assessments 36 (2019), 100560, https://doi.org/10.1016/j.seta.2019.100560.
[11] M. Ditaranto, T. Heggset, D. Berstad, Concept of hydrogen fired gas turbine cycle with exhaust gas recirculation: assessment of process performance, Energy 192 (2020), 116646, https://doi.org/10.1016/j.energy.2019.116646.
[12] A. Görgülü, H. Yağlı, Y. Koç, A. Koç, Comprehensive analysis of the effect of water injection on performance and emission parameters of the hydrogen fuelled recuperative and non-recuperative gas turbine system, Int. J. Hydrogen Energy 45 (58) (2020) 34254–34267, https://doi.org/10.1016/j.ijhydene.2020.09.038.
[13] Y. Koç, H. Yağlı, A. Görgülü, A. Koç, Analysing the performance, fuel cost and emission parameters of the 50 MW simple and recuperative gas turbine cycles using natural gas and hydrogen as fuel, Int. J. Hydrogen Energy (2020) 22138–22147, https://doi.org/10.1016/j.ijhydene.2020.05.267.
[14] T. Bexten, S. Jörg, N. Petersen, M. Wirsum, P. Liu, Z. Li, Model-based thermodynamic analysis of a hydrogen-fired gas turbine with external exhaust gas recirculation, in: Turbo Expo: Power for Land, Sea, and Air, vol. 84140, American Society of Mechanical Engineers, 2020, https://doi.org/10.1115/1.4049699.
[15] N.H. Petersen, T. Bexten, C. Goßrau, M. Wirsum, Analysis of the emission reduction potential and combustion stability limits of a hydrogen-fired gas turbine with external exhaust gas recirculation, in: Turbo Expo: Power for Land, Sea, and Air, vol. 84966, American Society of Mechanical Engineers, 2021, https://doi.org/10.1115/GT2021-58674.
[16] P. Chiesa, G. Lozza, L. Mazzocchi, Using hydrogen as gas turbine fuel, J. Eng. Gas Turbines Power 127 (1) (2005) 73–80, https://doi.org/10.1115/1.1787513.
[17] P. Gobbato, M. Masi, A. Toffolo, A. Lazzaretto, Numerical simulation of a hydrogen fuelled gas turbine combustor, Int. J. Hydrogen Energy 36 (13) (2011) 7993–8002, https://doi.org/10.1016/j.ijhydene.2011.01.045.
[18] S. Taamallah, K. Vogiatzaki, F.M. Alzahrani, E.M.A. Mokheimer, M.A. Habib, A.F. Ghoniem, Fuel flexibility, stability and emissions in premixed hydrogen-rich gas turbine combustion: technology, fundamentals, and numerical simulations, Appl. Energy 154 (2015) 1020–1047, https://doi.org/10.1016/j.apenergy.2015.04.044.
[19] A. Cappelletti, F. Martelli, Investigation of a pure hydrogen fueled gas turbine burner, Int. J. Hydrogen Energy 42 (15) (2017) 10513–10523, https://doi.org/10.1016/j.ijhydene.2017.02.104.
[20] A. Schastlivtsev, D. Dunikov, V. Borzenko, Experimental study of the processes in hydrogen-oxygen gas generator, Int. J. Hydrogen Energy. International Journal of Hydrogen Energy 44 (18) (2019) 9450–9455, https://doi.org/10.1016/j.ijhydene.2019.02.126.
[21] M. Nose, T. Kawakami, H. Araki, N. Senba, S. Tanimura, Hydrogen-fired gas turbine targeting realization of CO2-free Society, Mitsubishi Heavy Industries Technical Review 55 (4) (2018) 1–7. https://www.mhi.co.jp/technology/review/pdf/e554/e554180.pdf.
[22] N. Tekin, M. Ashikaga, A. Horikawa, H. Funke, Enhancement of fuel flexibility of industrial gas turbines by development of innovative hydrogen combustion systems, Gas Energy 2 (2018) 1–6. https://opus.bibliothek.fh-aachen.de/opus4/frontdoor/index/index/docId/8632.
[23] K.K. Lam, P. Geipel, J. Larfeldt, Hydrogen enriched combustion testing of siemens industrial SGT-400 at atmospheric conditions, J. Eng. Gas Turbines Power 137 (2015) 2, https://doi.org/10.1115/1.4028209.
[24] M. Balestri, G. Benelli, F. Donatini, F. Arlati, G. Conti, Enel's Fusina hydrogen-fed power generation plant, in: International Conference on Clean Electrical Power, vol. 2007, IEEE, 2007, pp. 456–463, https://doi.org/10.1109/ICCEP.2007.384254.
[25] T.K. Tromp, R.L. Shia, M. Allen, J.M. Eiler, Y.L. Yung, Potential environmental impact of a hydrogen economy on the stratosphere, Science 300 (5626) (2003) 1740–1742, https://doi.org/10.1126/science.1085169.

[26] Y. Yang, Z. Bai, G. Zhang, Y. Li, Z. Wang, G. Yu, Design/off-design performance simulation and discussion for the gas turbine combined cycle with inlet air heating, Energy 178 (2019) 386–399, https://doi.org/10.1016/j.energy.2019.04.136.
[27] S.H. Cha, S.I. Na, Y.H. Lee, M.S. Kim, Thermodynamic analysis of a gas turbine inlet air cooling and recovering system in gas turbine and CO2 combined cycle using cold energy from LNG terminal, Energy Convers. Manag. 230 (2021), 113802, https://doi.org/10.1016/j.enconman.2020.113802.
[28] X. Liu, X. Gao, X. Wu, W. Yu, L. Chen, R. Ni, Y. Zhao, H. Duan, F. Zhao, L. Chen, S. Gao, K. Xu, J. Lin, A.Y. Ku, Updated Hourly emissions factors for Chinese power plants showing the impact of widespread ultralow emissions technology deployment, Environ. Sci. Technol. 53 (5) (2019) 2570–2578, https://doi.org/10.1021/acs.est.8b07241.
[29] K. Mohammadi, M. Saghafifar, J.G. McGowan, Thermo-economic evaluation of modifications to a gas power plant with an air bottoming combined cycle, Energy Convers. Manag. 172 (2018) 619–644, https://doi.org/10.1016/j.enconman.2018.07.038.
[30] P. Pourmoghadam, M. Farighi, F. Pourfayaz, et al., Annual transient analysis of energetic, exergetic, and economic performances of solar cascade organic Rankine cycles integrated with PCM-based thermal energy storage systems, Case Stud. Therm. Eng. 28 (2021), 101388, https://doi.org/10.1016/j.csite.2021.101388.
[31] Z. Cesaro, M. Ives, R. Nayak-Luke, et al., Ammonia to power: forecasting the levelized cost of electricity from green ammonia in large-scale power plants, Appl. Energy 282 (2021), 116009, https://doi.org/10.1016/j.apenergy.2020.116009.
[32] IEA, Energy Technology Perspectives, Special Report on Clean Energy Innovation, Energy Technol. Perspect. 2020, 2020, p. 2020. http://119.78.100.173/C666/handle/2XK7JSWQ/283485.
[33] S.P.A. Brown, M.K. Yücel, What drives natural gas prices? Energy J. 29 (2008) 2, https://doi.org/10.5547/ISSN0195-6574-EJ-Vol29-No2-3.
[34] A. Hailemariam, R. Smyth, What drives volatility in natural gas prices? Energy Econ. 80 (2019) 731–742, https://doi.org/10.1016/j.eneco.2019.02.011.
[35] C. Hendriks, W. Graus, F. van Bergen, Global Carbon Dioxide Storage Potential and Costs, vol. 64, Ecofys, Utr, 2004. https://www.osti.gov/etdeweb/biblio/20464118.
[36] G. Brändle, M. Schönfisch, S. Schulte, Estimating long-term global supply costs for low-carbon hydrogen, Appl. Energy 302 (2021), 117481, https://doi.org/10.1016/j.apenergy.2021.117481.
[37] M. Bui, C.S. Adjiman, A. Bardow, E.J. Anthony, A. Boston, S. Brown, P.S. Fennell, S. Fuss, A. Galindo, L.A. Hackett, J.P. Hallett, H.J. Herzog, G. Jackson, J. Kemper, S. Krevor, G.C. Maitland, M. Matuszewski, I.S. Metcalfe, C. Petit, G. Puxty, J. Reimer, D.M. Reiner, E.S. Rubin, S.A. Scott, N. Shah, B. Smit, J.P. M. Trusler, P. Webley, J. Wilcox, N. Mac Dowell, Carbon capture and storage (CCS): the way forward, Energy Environ. Energy & Environmental Science 11 (5) (2018) 1062–1176, https://doi.org/10.1039/c7ee02342a.
[38] R.S. El-Emam, H. Özcan, Comprehensive review on the techno-economics of sustainable large-scale clean hydrogen production, J. Clean. Prod. 220 (2019) 593–609, https://doi.org/10.1016/j.jclepro.2019.01.309.
[39] J. Chi, H. Yu, Water electrolysis based on renewable energy for hydrogen production, Chin. J. Catal. 39 (3) (2018) 390–394, https://doi.org/10.1016/S1872-2067(17)62949-8.
[40] B. Hrnčić, A. Pfeifer, F. Jurić, et al., Different investment dynamics in energy transition towards a 100% renewable energy system, Energy 237 (2021), 121526, https://doi.org/10.1016/j.energy.2021.121526.
[41] Z. Wang, H. Chen, S. Weng, Revised Dalton's method for calculation of thermodynamic properties of unsaturated humid air and gas mixture after combustion in humid air turbine cycle, Energy 58 (2013) 594–605, https://doi.org/10.1016/j.energy.2013.05.049.
[42] J. Graetz, New approaches to hydrogen storage, Chem. Soc. Rev. 38 (1) (2009) 73–82, https://doi.org/10.1039/b718842k.
[43] S. Hosseinimaab, A. Tousi, A new approach to off-design performance analysis of gas turbine engines and its application, Energy Convers. Manag. 243 (2021), 114411, https://doi.org/10.1016/j.enconman.2021.114411.
[44] S. Yee, J. Milanovic, F. Hughes, Overview and comparative analysis of gas turbine models for system stability studies, IEEE Trans. Power Syst. 23 (2008) 108–118, https://doi.org/10.1109/TPWRS.2007.907384.
[45] Z. Al-Hamdan Q, M. Ebaid, Modeling and simulation of a gas turbine engine for power generation, J. Eng. Gas Turbines Power 128 (2006) 302–311, https://doi.org/10.1115/1.2061287.
[46] J. Deng, F. Liang, Y. Ding, Z. Yang, G. Xu, J. Liu, Performance analysis of induced draft fan driven by steam turbine for 1000 MW power units, Energy Power Eng. 5 (4) (2013) 1387, https://doi.org/10.4236/epe.2013.54b263.

Nomenclature

π: pressure ratio
n: rotating speed (rpm)
G: mass flow rate (kg/s)
t: temperature (K)
p: pressure (kPa)
Δhs: isentropic enthalpy difference (kJ/kg)
h: enthalpy (kJ/kg)
P: power (kW)
C_p*:* specific heat at constant pressure [J/(kg·K)]
LHV: lower heating value (kJ/kg)
Q: heat *exchange* amount (W)
LnD: logarithmic mean temperature difference
$\triangle t$*:* temperature difference (K)
k: heat transfer coefficient [W/(m2·K)]
A: heat transfer area (m2)
*dtapp: tem*perature difference at the approach point (K)
d: moisture content (kg/kgda)
pv: water vapor partial pressure (Pa)
pa: air pressure (Pa)
GSC: standard coal equivalent (kg/s)
LCOE: levelized cost of electricity ($/MWh)
I: levelized investment cost of electricity ($)
F: levelized fuel cost of electricity ($)
Em: levelized emission cost of electricity ($)
M: levelized maintenance cost of electricity ($)
ELE: electricity quantity produced by gas turbine combined cycle (W)
OT: operating time (year)
c: cost ($)
Pr: price of CO_2($/kg)

Greek symbols

η: efficiency (%)

l: air–fuel ratio
α: total pressure recovery coefficient
ηel: power generation efficiency of generator (%)
*ηm: mech*anical efficiency (%)

Subscripts

C: compressor
1: compressor inlet
2: compressor outlet
f: fuel
3: turbine inlet
4: turbine outlet
0: standard condition
T: turbine
hf: hot fluid of heat exchanger
': at the inlet
'': at the outlet
cf: cold fluid of heat exchanger
EC: economizer
EV: evaporator
SH: superheater
SA: saturated steam
*gen: produce*d by generator
shaft: shaft power
p: pump
mix1,2,3: 1st inlet, 2nd inlet, and outlet fluids of mixer
spl1,2,3: 1st inlet, 2nd inlet, and outlet fluids of splitter
WRC: water recovery condenser
CW: condensed water
GTCC: gas turbine combined cycle
GT: gas turbine
ST: steam turbine
NG: natural gas
H2: hydrogen
CO2: carbon dioxide
y: in year y
total: total cost
t: in 1 year
ivm: investment
trans: transportation
d: transportation distance
ccs: captured CO2 emission
ue: uncaptured CO2 emission
mnt: maintenance
HPT: high-pressure turbine
IPT: intermediate-pressure turbine
LPT: low-pressure turbine
ES: exhaust steam from low-pressure steam turbine
HS: steam extraction from the steam turbine for heat supply
EG: exhaust gas
EGB: exhaust gas blower
Net: difference between the produced power and the consumed power

Abbreviations

GTCC: gas turbine combined cycle
GT: gas turbine
SO2: sulfur dioxide
NOx: nitrogen oxides
DLE: dry low emissions
CO2: carbon dioxide
EGR: exhaust gas recirculation
*CC: combus*tion chamber
HRSG: heat recovery steam generator
WRC: water recovery condenser
EGB: exhaust gas blower
HPT: high-pressure turbine
IPT: intermediate-pressure turbine
*LPT: low-pres*sure turbine